



Molybdenum doped spinel as cathode material for lithium rechargeable cells

R. Thirunakaran^{a,*}, R. Ravikumar^a, S. Vijayarani^b, S. Gopukumar^a, A. Sivashanmugam^a

^a Central Electrochemical Research Institute, Karaikudi 630 006, Tamil Nadu, India

^b Vivekanandha College of Arts & Sciences for Women, Elayampalayam, Tiruchengode, Tamil Nadu, India

ARTICLE INFO

Article history:

Received 14 June 2010

Received in revised form 28 August 2011

Accepted 31 August 2011

Available online 8 October 2011

Keywords:

B. Intercalation reaction

D. Electrochemical properties

B. Sol–gel chemistry

C. X-ray diffraction

D. Energy storage

ABSTRACT

Spinel $\text{LiMo}_x\text{Mn}_{2-x}\text{O}_4$ ($x = 0.01, 0.05, 0.10$) samples are synthesized using solid state technique and characterized by thermo gravimetric analysis (TG/DTA), X-ray diffraction (XRD), Fourier transform infrared spectroscopy (FT-IR), scanning electron microscopy (SEM), transmission electron microscopy (TEM) and galvanostatic cycling studies. Thermal studies depict that the formation of spinel compound proceeds in three stages. XRD peak reflections point out the formation of spinel phase. SEM studies confirm that $\text{LiMo}_{0.01}\text{Mn}_{1.99}\text{O}_4$ calcined at 850°C are of $1\ \mu\text{m}$ grains. Among the dopant concentrations investigated, $\text{LiMo}_{0.01}\text{Mn}_{1.99}\text{O}_4$ sample shows better cycling characteristics. $\text{LiMo}_{0.01}\text{Mn}_{1.99}\text{O}_4$ spinel delivers a maximum discharge capacity of $66\ \text{mA}\ \text{hg}^{-1}$ during the first cycle corresponding to coulombic efficiency of 84% and exhibits a capacity fade of $0.2\ \text{mA}\ \text{hg}^{-1}\ \text{cycle}^{-1}$ over the investigated 10 cycles.

© 2011 Published by Elsevier Ltd.

1. Introduction

Pristine spinel LiMn_2O_4 is one of the most attractive candidates for rechargeable lithium batteries due to its low cost, non-toxic nature and ease of preparation when compared with other layered oxides such as LiCoO_2 and LiNiO_2 [1–3]. LiCoO_2 has many disadvantages such as high cost, toxic and low practical specific capacity. The capacity of pure spinel LiMn_2O_4 diminishes at elevated temperature upon repeated cycling [4,5]. The capacity fading is caused due to several factors such as Jahn–Teller distortion, two-phase unstable reaction [2], slow dissolution of manganese into the electrolyte [6], lattice instability [7], and particle size distribution [8,9]. In order to suppress Jahn–Teller distortion for obtaining high cycling capacity, many researchers have studied lithium rich spinels with various divalent, trivalent and tetravalent-doped ions such as Co, Zn, Cu, Fe, Ni, Cr, Ga, Ti and Al [10]. Ohzuku et al. [8] and Lee et al. [11] have reported that partial doping of divalent and trivalent cations are more effective in suppressing the capacity fade upon cycling. Furthermore, the capacity fade of LiMn_2O_4 is often observed much in 3 V region which can be completely suppressed by doping of LiMn_2O_4 by multivalent cations [12]. Several low temperature preparation methods viz., sol–gel method [13,14], chemical precipitation [15] Pechini process and hydrothermal [16], ultrasonic spray pyrolysis method [17] have been employed to obtain cathode materials of required physical and electrochemical properties for lithium-ion-batteries.

In the present investigation, an attempt has been made to synthesize Mo-doped LiMn_2O_4 spinel via solid state method. The oxidation state of molybdenum is Mo^{5+} in this spinel compound. Also, molybdenum has larger ionic radius ($0.65\ \text{\AA}$) than the Mn^{4+} and Mn^{3+} ions which are measuring 0.53 and $0.58\ \text{\AA}$, respectively. Doping with larger dopant ions is found to be beneficial in achieving stable cycling performance. Several multivalent dopants like Ni ($0.69\ \text{\AA}$), Fe ($0.645\ \text{\AA}$), Co ($0.745\ \text{\AA}$) etc., have been widely investigated to stabilize the spinel structure. Furthermore, there is no literature available on thermal synthesis of Mo-doped spinel compound.

2. Experimental

$\text{LiMo}_x\text{Mn}_{2-x}\text{O}_4$ ($x = 0.01, 0.05, 0.10$) powders have been synthesized by solid state technique. Fig. 1 depicts the flow chart of the solid state synthesis. Stoichiometric amounts of carbonates of lithium, manganese and molybdenum oxide were thoroughly mixed and ground well for obtaining homogeneity. The ground homogenized precursors are calcined at different temperatures [18]. A portion of this compound has been taken for TG/DTA analysis to understand the thermal behaviour and the rest of the sample was calcined at 850°C for 12 h. The calcined samples are subjected to various physical (XRD, SEM, TEM, FT-IR) characterization and galvanostatic charge/discharge cycling studies.

2.1. Coin cell fabrication

Coin cells of 2016 configuration have been assembled in an argon filled glove box (MBraun, Germany) using lithium foil as

* Corresponding author. Fax: +91 4565 227779.

E-mail address: rthirunakaran@yahoo.com (R. Thirunakaran).

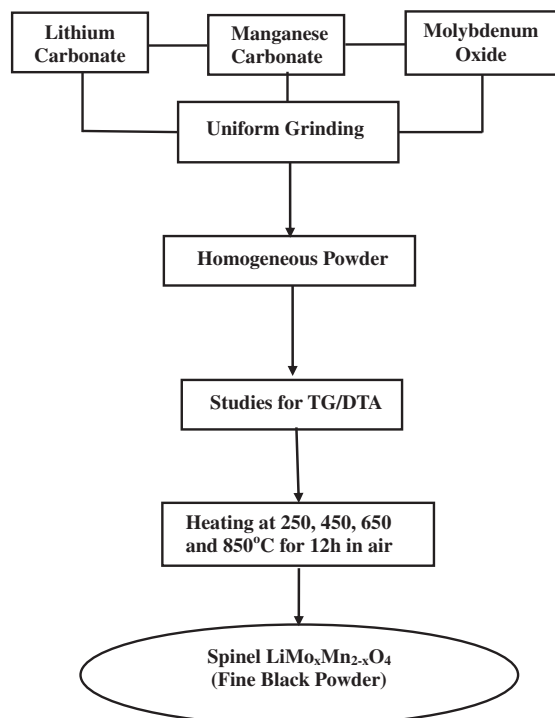


Fig. 1. Flow chart for synthesis of $\text{LiMo}_x\text{Mn}_{2-x}\text{O}_4$ by solid-state method.

anode, Celgard 2400 as separator, 1 M solution of LiPF_6 in 50:50 (v/v) mixture of ethylene carbonate (EC) and diethylene carbonate (DEC) as electrolyte and the synthesized material as cathode. The

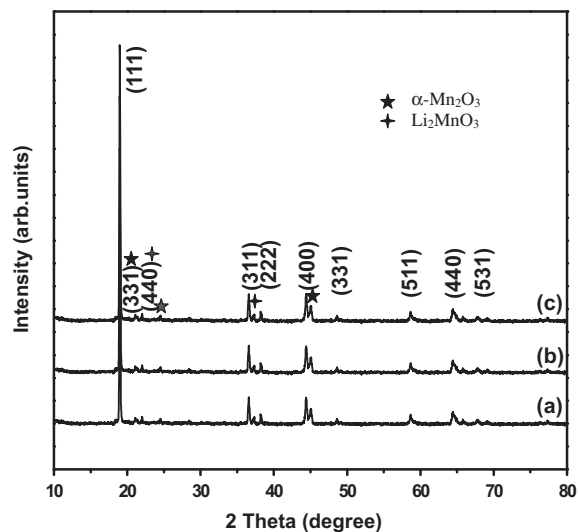


Fig. 3. XRD patterns of $\text{LiMo}_x\text{Mn}_{2-x}\text{O}_4$ calcined at 850 °C (a) $x = 0.01$; (b) $x = 0.05$; (c) $x = 0.10$.

cathode is prepared by a slurry coating procedure from a mix comprising synthesized compound, carbon black and poly vinylidene fluoride (PVdF) binder in *n*-methyl-2-pyrrolidone (NMP) solution mixed in the ratio 80:10:10 so as to form slurry. The slurry has been coated over aluminium foil and vacuum dried at 110 °C for 2 h. The dried coating is pressed at an optimized pressure of 680 kg cm^{-1} for 2 min. Electrode blanks of 18 mm diameter are punched out and used as a cathode in the coin cell.

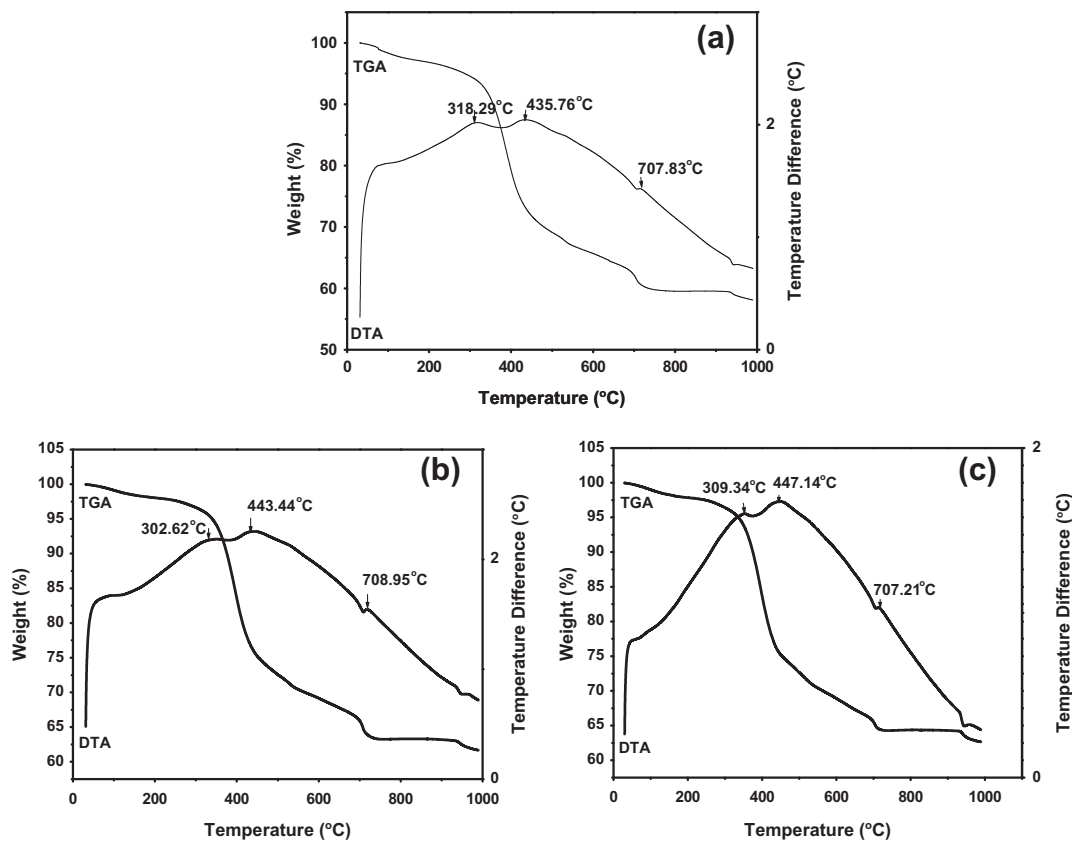


Fig. 2. Thermo gravimetric and differential thermal analysis of $\text{LiMo}_x\text{Mn}_{2-x}\text{O}_4$ spinel precursor. (a) $x = 0.01$; (b) $x = 0.05$; (c) $x = 0.10$.

Table 1
Unit cell parameters and crystallite size of $\text{LiMo}_x\text{Mn}_{2-x}\text{O}_4$ spinels calcined at 850 °C for 12 h.

No.	Sample	a (Å)	Unit cell volume (Å) ³	Crystallite size $\times 10^{-9}$ m
1	$\text{LiMo}_{0.01}\text{Mn}_{1.99}\text{O}_4$	8.2273	556	20.60
2	$\text{LiMo}_{0.05}\text{Mn}_{1.95}\text{O}_4$	8.2126	553	21.70
3	$\text{LiMo}_{0.10}\text{Mn}_{1.90}\text{O}_4$	8.2394	559	22.40

Table 2
Observed XRD data for $\text{LiMo}_x\text{Mn}_{2-x}\text{O}_4$ spinels.

S. No.	Sample	2θ	d (Å) Obs.	I/I_0	hkl	Plane intensity
1	$\text{LiMo}_{0.01}\text{Mn}_{1.99}\text{O}_4$	19.0	4.67265	3.1	111	100
2	$\text{LiMo}_{0.05}\text{Mn}_{1.95}\text{O}_4$	19.0	4.67061	3.0	111	100
3	$\text{LiMo}_{0.10}\text{Mn}_{1.90}\text{O}_4$	19.2	4.67297	1.2	111	100

2.2. Electrochemical studies

The coin cells are subjected to constant current charge–discharge cycling studies at C/10 rate between 3.0 and 4.5 V using an in-house battery cycling unit. Differential capacity curves are plotted using the charge–discharge cycling data to understand the real time electrochemical sequence.

3. Results and discussion

3.1. Thermal studies

Fig. 2 shows TG/DTA curves of $\text{LiMo}_x\text{Mn}_{2-x}\text{O}_4$ ($x = 0.01, 0.05, 0.10$) synthesized via solid state method. The TG curve (Fig. 2a) exhibits a cumulative weight loss of about 42% spreading over

three zones. A trace of 3% weight loss appears around 100 °C is owing to the removal of residual water molecule present in the precursors. The first weight loss zone (8%) is extending up to 350 °C followed by the second sharp fall region (30%) appearing till 700 °C. The third weight loss zone is measuring 4% and becoming flat beyond 730 °C indicating the ending of the thermal event. The whole process appears as a single broad exothermic event in the DTA curve with peak centers at 318, 435 and 707 °C which may be ascribed to the decomposition of the precursors. The formation of spinel compound occurs at around 435 °C and the heating process extending till 800 °C may be attributed to the crystal structural refinement around the grain boundaries. TG/DTA profiles of doped spinel compounds prepared by other synthesis procedures [19–21] also exhibiting similar behaviour with regard to the formation temperature. The TG/DTA profiles of all the samples (Fig. 2b and c) exhibit similar behaviour with a very little difference in the peak temperatures.

3.2. X-ray diffraction studies

Fig. 3 depicts the XRD patterns of $\text{LiMo}_x\text{Mn}_{2-x}\text{O}_4$ with different stoichiometric amounts of molybdenum metal cations viz., (a) Mo = 0.01; (b) Mo = 0.05; (c) Mo = 0.10 synthesized via thermal

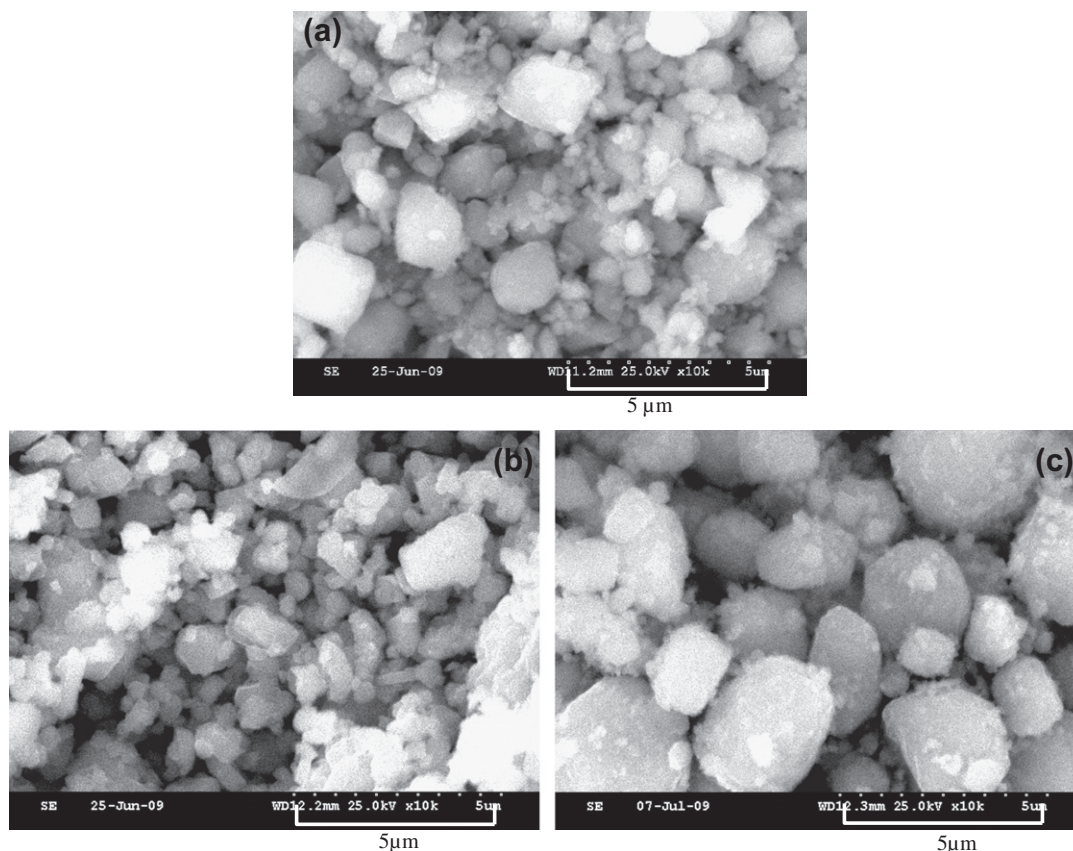


Fig. 4. SEM images of $\text{LiMo}_x\text{Mn}_{2-x}\text{O}_4$ spinel particles calcined at 850 °C (a) $x = 0.01$; (b) $x = 0.05$; (c) $x = 0.10$.

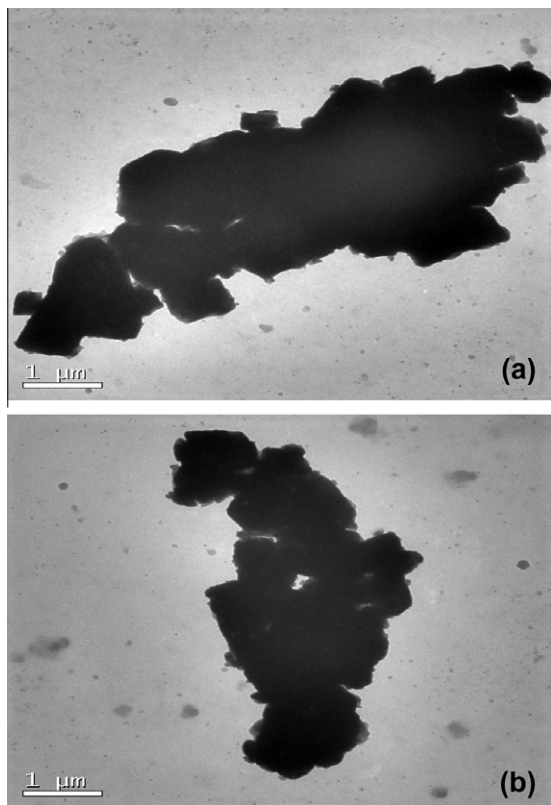


Fig. 5. TEM images of spinel $\text{LiMo}_x\text{Mn}_{2-x}\text{O}_4$ particles calcined at 850°C (a) $x = 0.01$; (b) $x = 0.10$.

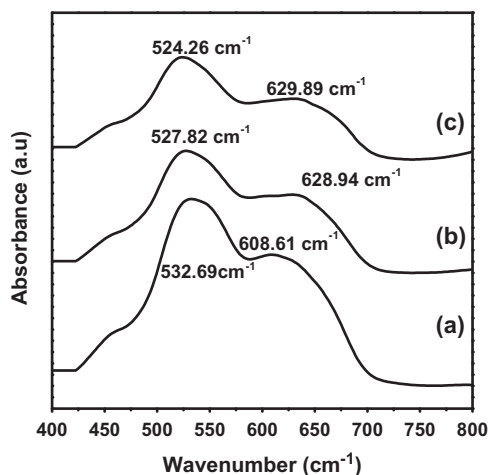


Fig. 6. FT-IR Spectra of $\text{LiMo}_x\text{Mn}_{2-x}\text{O}_4$ particles with varying Mo-doping calcined at 850°C (a) $x = 0.01$; (b) $x = 0.05$; (c) $x = 0.10$.

method calcined at 850°C . All the XRD peak reflections perfectly match with JCPDS card. No. 35–782. It is evident from the matching spectral profiles corresponding to the planes (111), (331), (440), (311), (222), (400), (511), (440) and (531) for the $\text{LiMo}_x\text{Mn}_{2-x}\text{O}_4$ samples indicate the formation of highly crystalline spinel phase. However, few impurity peaks of $\alpha\text{-Mn}_2\text{O}_3$ and Li_2MnO_3 are also seen corresponding to the planes (331) and (440). The crystallite size for the $\text{LiMo}_x\text{Mn}_{2-x}\text{O}_4$ compounds has been calculated using Debye–Scherrer equation and the crystallites are around ~ 20 nm size [22]. Table 1 shows the unit cell parameters and crystallite size of the spinel $\text{LiMo}_x\text{Mn}_{2-x}\text{O}_4$ compounds. It

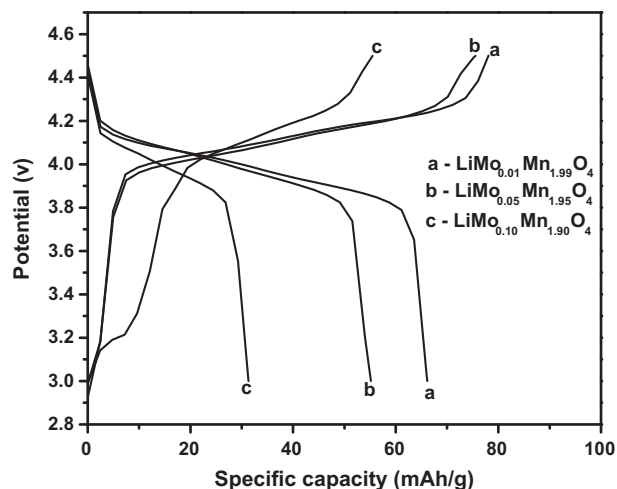


Fig. 7. First cycle charge–discharge behaviour of $\text{LiMo}_x\text{Mn}_{2-x}\text{O}_4$ with varying Mo-doping viz., 0.01, 0.05, and 0.10 calcined at 850°C .

can be seen that with increase in Mo-doping the crystallite size increases and with regard to the unit cell parameter the variations are not definable. Table 2 shows the observed XRD data for $\text{LiMo}_x\text{Mn}_{2-x}\text{O}_4$ spinels. Lesser the I/I_0 value indicates high order of cation mixing there by resulting to poor structural stability. This is reflected in the cycling performance wherein higher Mo-doping shows poor electrochemical behaviour.

3.3. SEM and TEM analyses

SEM studies ascertain the surface morphology of the compound. Fig. 4 shows SEM images of $\text{LiMo}_x\text{Mn}_{2-x}\text{O}_4$ spinel powders (a) Mo = 0.01; (b) Mo = 0.05; (c) Mo = 0.10. The grains (Fig. 4a) of Mo-doped ($x = 0.01$) spinel are of globular morphology with an average grain size of ~ 1 μm . Further, it can be seen that $\text{LiMo}_{0.05}\text{Mn}_{1.95}\text{O}_4$ compounds have relatively smaller grains with poor agglomeration and the average particle size is around 1 μm (Fig. 4b). In the case of $\text{LiMo}_{0.10}\text{Mn}_{1.90}\text{O}_4$ (Fig. 4c), the grains are rather bigger i.e., ~ 3 μm . However, a small percentage of 1 μm particles are also present. $\text{LiMo}_{0.01}\text{Mn}_{1.99}\text{O}_4$ particles with smaller grain size and globular morphology could be beneficial so as to derive better electrochemical performance. Fig. 5 shows the TEM images of $\text{LiMo}_x\text{Mn}_{2-x}\text{O}_4$ (a) Mo = 0.01; (b) Mo = 0.10. Both samples present as non agglomeratives with unit grain size around 1 μm .

3.4. FTIR spectroscopy

Fig. 6 depicts FT-IR spectra of $\text{LiMo}_x\text{Mn}_{2-x}\text{O}_4$ powders (a) Mo = 0.01; (b) Mo = 0.05; (c) Mo = 0.10. The FTIR spectra exhibit two absorption peaks. The reflection around $524\text{--}532$ cm^{-1} may be assigned to Li–O bending vibration and the spectral reflections seen at higher wave number between 608 and 629 cm^{-1} corresponds to Li–Mo–Mn–O stretching vibration. It is apparent that with increasing dopant concentration the peaks become broader and getting separated. Also, the peak reflection of low Mo-doped spinel (0.01) appears at lower wave number than higher Mo-doped ones (0.05, 0.10). These characteristics are in good agreement with earlier reports [23–25].

3.5. Charge–discharge studies

Fig. 7 depicts the charge–discharge behaviour of $\text{LiMo}_x\text{Mn}_{2-x}\text{O}_4$ particles during the first cycle. Charge–discharge curves lucidly

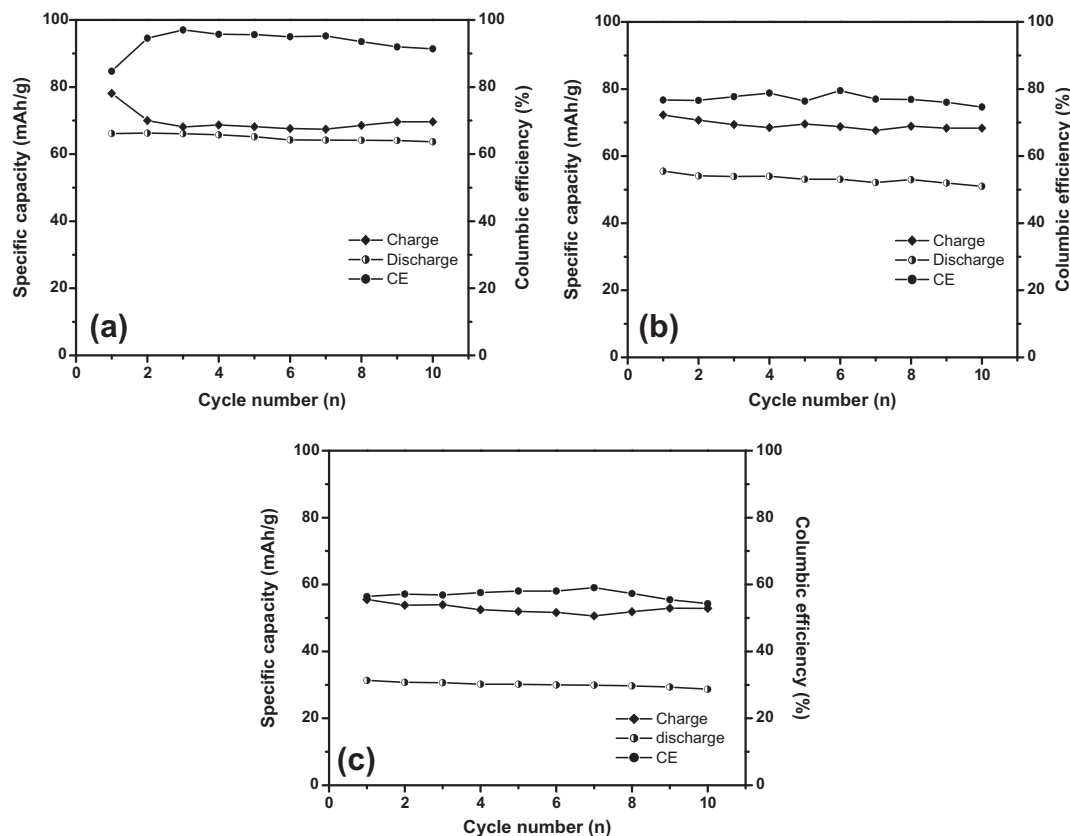


Fig. 8. Cyclic behaviour of $\text{LiMo}_x\text{Mn}_{2-x}\text{O}_4$ with varying Mo-doping viz., 0.01, 0.05, and 0.10 calcined at 850°C .

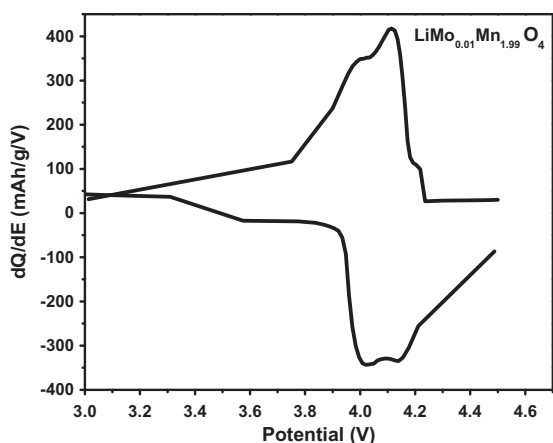


Fig. 9. dQ/dE vs. potential curves of $\text{LiMo}_{0.01}\text{Mn}_{1.99}\text{O}_4$.

show a clear plateau region suggesting deintercalation and intercalation process. It is evident that with increase in the dopant content a slight decrease in capacity has been observed. Mo-doped spinels (0.01, 0.05, 0.10) deliver discharge capacities of 66, 55 and 31 mA hg^{-1} during the first cycle which corresponds to a coulombic efficiency of 84%, 74% and 54%, respectively. Fig. 8 shows the cycling performance of $\text{LiMo}_x\text{Mn}_{2-x}\text{O}_4$ particles and the coulombic efficiency. Mo-doped (0.01, 0.05, 0.10) spinels exhibits maximum discharge capacity of 64, 51 and 30 mA hg^{-1} corresponding to a coulombic efficiency of 84%, 74% and 54% respectively in the 10th cycle. It is apparent that $\text{LiMo}_{0.01}\text{Mn}_{1.99}\text{O}_4$ particles out performs the other compositions and the high Mo-doped sample exhibit extremely poor performance. A close observation on the charging profile in

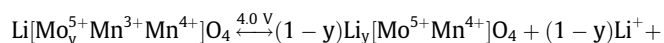
the case of $\text{LiMo}_{0.1}\text{Mn}_{1.9}\text{O}_4$ shows a small plateau around 3 V which may be attributed to the Jahn–Teller active zone which eventually leads to poor electrochemical performance and high fading behaviour. Over the investigated 10 cycles Mo-doped (0.01, 0.05, 0.10) spinels exhibits a capacity fade of 0.2, 0.4 and $0.3 \text{ mA hg}^{-1} \text{ cycle}^{-1}$, respectively. Meanwhile, a comparison of electrochemical performance of pristine spinel LiMn_2O_4 prepared via solid state method [26–28] with that of Mo-doped ones, the former delivers an initial specific capacity of $\sim 120 \text{ mA hg}^{-1}$ while they exhibit fading cycling performance. In contrast, Mo-doped spinel compounds exhibit comparatively low discharge capacity but Mo-doped spinel ($x = 0.01$) exhibits stable cycling performance with high capacity retention characteristics. Indeed, the high reversible capacity that has been obtained with Mo-doped spinel upon cycling may be attributed to its higher ionic radius (0.65 Å) while the same for Mn^{4+} and Mn^{3+} ions are measuring 0.53 and 0.58 Å respectively. It is also worth mentioning that higher ionic radii of dopant metal cations like Ce: 1.034 Å and Zn: 0.7 Å are higher than Mn-ions have delivered stable cycling performance [23]. Further more, it is obvious that the discharge capacity even during the first cycle is much varied among the varying dopant concentration. The genuine reason may be due to the formation of secondary phases on the surface of the spinel particles that make barrier effect between the LiMn_2O_4 particles and electrolyte. On the other hand, high Mo-doped spinel shows a modest change in unit cell parameter leading to a slight volume change which stands as evidence for possible structural deformation at higher concentration.

Low Mo-doped spinel ($\text{LiMo}_{0.01}\text{Mn}_{1.99}\text{O}_4$) delivers slightly superior capacity of 66 mA hg^{-1} during the first cycle and exhibits 64 mA hg^{-1} at the end of the 10th cycle. It is not ruled out that a low order of cation distribution into the manganese site also stabilizes the spinel structure [23]. A comparison of these results with an earlier study [17] on Mo-doped spinel synthesized via spray

pyrolysis reveals that Mo-doping has been found to be beneficial and further stable electrochemical performance has been realized from low degree of Mo-doped ($x=0.02$) samples. Though, in the present study, the capacity obtained from the Mo-doped spinel products are relatively lower the overall characteristics are in good agreement with that of earlier literature that Mo-doping essentially improves the cycling characteristics. Hence, low level of Mo-doping on spinel structure exhibits better cycling behaviour and good capacity retention.

3.6. dQ/dE vs. potential curves

Fig. 9 depicts the differential capacity curve for $\text{LiMo}_{0.01}\text{Mn}_{1.99}\text{O}_4$ which mimic the true electrochemical sequence. It is lucidly seen that the two anodic and cathodic peaks at around 4 and 4.11 V corresponds to deintercalation process for lithium ion extraction at 8a tetrahedral sites where Li occupies associated with $\text{Mn}^{3+}/\text{Mn}^{4+}$, $\text{Mo}^{5+}/\text{Mo}^{6+}$ couples. The possible electrochemical reaction may be represented as follows:



4. Conclusions

$\text{LiMo}_x\text{Mn}_{2-x}\text{O}_4$ ($x = 0.01, 0.05, 0.10$) have been synthesized for the first time via solid state method to use as a cathode material in lithium rechargeable batteries. XRD peak signatures of $\text{LiMo}_x\text{Mn}_{2-x}\text{O}_4$ exhibit high degree of crystallinity and phase purity. SEM and TEM images of $\text{LiMo}_{0.01}\text{Mn}_{1.99}\text{O}_4$ calcined at 850 °C lucidly depict that the grains are of 1 μm size. Among the dopant concentrations investigated, $\text{LiMo}_{0.01}\text{Mn}_{1.99}\text{O}_4$ sample shows better cycling characteristics. Charge–discharge studies of $\text{LiMo}_{0.01}\text{Mn}_{1.99}\text{O}_4$ spinel delivers a maximum discharge capacity of 66 mA hg^{-1} during the first cycle corresponding to coulombic efficiency of 84% and exhibits a capacity fade of 0.2 mA hg^{-1} cycle $^{-1}$ over the investigated 10 cycles.

Acknowledgment

The authors gratefully acknowledge the support given under the Indo-Taiwan collaborative research programme.

References

- [1] Tarascon JM, McKinnon WR, Coowar F, Bowner TN, Amatucci G, Guyomard D. *J Electrochem Soc* 1994;141:1421–31.
- [2] Gummow RJ, de Kock A, Thackeray MM. *Solid State Ionics* 1994;69:59–67.
- [3] Thackeray MM, de Kock A, Rossouw MH, Liles D, Bittihn R, Hoge D. *J Electrochem Soc* 1992;139:363–6.
- [4] Xia Y, Yoshio M. *J Electrochem Soc* 1977;144:2593–600.
- [5] Pistoia G, Antonini A, Rosati R, Zane D. *Electrochim Acta* 1996;41:2683–9.
- [6] Jang DH, Shin JY, Oh SM. *J Electrochem Soc* 1996;143:2204–11.
- [7] Yamada A. *J Solid State Chem* 1996;122:160–5.
- [8] Ohuzuku T, Takeda S, Iwanaga M. *J Power Sources* 1999;81:90–4.
- [9] Song D, Ikuta H, Uchida T, Wakihara M. *Solid State Ionics* 1999;117:151–6.
- [10] Javed Iqbal M, Zahoor S. *J Power Sources* 2007;165:393–7.
- [11] Lee JH, Hong JK, Jang DH, Sun YK, Oh SM. *J Power Sources* 2000;89:7–14.
- [12] Park SH, Park KS, Sun YK, Nahm KS. *J Electrochem Soc* 2000;147:2116–21.
- [13] Bach S, Henry M, Baffier N, Livage J. *J Solid State Chem* 1990;88:325–33.
- [14] Perreira-Ramos JP. *J Power Sources* 1995;54:120–6.
- [15] Barboux P, Tarascon JM, Shokoohi FK. *J Solid State Chem* 1991;94:185–96.
- [16] Liu W, Farrington GC, Chaput F, Dunn BJ. *J Electrochem Soc* 1996;143:879–84.
- [17] Park SH, Oh SW, Myung ST, Sun YK. *Electrochem Solid-State Lett* 2004;7:A451–4.
- [18] Thirunakaran R, Kalaiselvi N, Periasamy P, Ramesh Babu B, Renganathan NG, Muniyandi N, et al. *Ionics* 2001;7:187–91.
- [19] Hwang BJ, Santhanam R, Liu DG. *J Power Sources* 2001;101:86–9.
- [20] Lee Byeong Woo. *J Power Sources* 2002;109:220–6.
- [21] Cha-Qing XU, Yan-wen TIAN, Yu-chun ZHAI, Bing YU, Zhao-jing GUO. *Trans Nonferrous Met Soc China* 2004;470–4.
- [22] Shaheen WM. *Thermochim Acta* 2002;385:105–16.
- [23] Thirunakaran R, Sivashanmugam A, Gopukumar S, Rajalakshimi R. *J Power Sources* 2009;187:565–74.
- [24] Thirunakaran R, Sivashanmugam A, Gopukumar S, Dunnill Charles W, Gregory Duncan H. *J Phys Chem Solids* 2008;69:2082–90.
- [25] Pimentel PM, Martinelli AE, Araujo Melo De Maria de, Garrido Pedrosa AM, Junha JD, Silva Jr CN. *Mater Res* 2005;8:9.
- [26] Gadjov H, Gorova M, Kotzeva V, Avdeev G, Uzunova S, Kovacheva D, et al. *J Power Sources* 2004;134:110–7.
- [27] Wan Chuanyun, Nuli Yanna, Zhuang Jihua, Jiang Zhiyu. *Mat Lett* 2002;56:357.
- [28] Tao Li, Weihua Qiu, Hailei Zhao, Jingjing Liu. *Mat Lett* 2006;60:1251.